



Cite this: *Chem. Sci.*, 2018, 9, 6785

All publication charges for this article have been paid for by the Royal Society of Chemistry

Synthesis and structural characterization of inverse-coordination clusters from a two-electron superatomic copper nanocluster†

Kiran Kumarvarma Chakrahari,^a Rhone P. Brocha Silalahi,^a Jian-Hong Liao,^a Samia Kahlal,^b Yu-Chiao Liu,^c Jyh-Fu Lee,^d Ming-Hsi Chiang,^c Jean-Yves Saillard^b and C. W. Liu^a

We have synthesized and structurally characterized a series of centred cuboctahedral copper clusters, namely $[\text{Cu}_{13}(\text{S}_2\text{CNR}_2)_6(\text{C}\equiv\text{CR}')_4](\text{PF}_6)$, **1a–d** (where **a**: $\text{R} = \text{tBu}$, $\text{R}' = \text{CO}_2\text{Me}$; **b**: $\text{R} = \text{tBu}$, $\text{R}' = \text{CO}_2\text{Et}$; **c**: $\text{R} = \text{iPr}$, $\text{R}' = \text{CO}_2\text{Et}$; **d**: $\text{R} = \text{nPr}$, $\text{R}' = 3,5\text{-(CF}_3)_2\text{C}_6\text{H}_3$); $[\text{Cu}_{12}(\mu_{12}\text{-S})(\text{S}_2\text{CNR}_2)_6(\text{C}\equiv\text{CR}')_4]$, **2a–c**; $[\text{Cu}_{12}(\mu_{12}\text{-Cl})(\text{S}_2\text{CNR}_2)_6(\text{C}\equiv\text{CR}')_4](\text{PF}_6)$, **3a–e** (where **e**: $\text{R} = \text{tBu}$, $\text{R}' = \text{Ph}$); $[\text{Cu}_{12}(\mu_{12}\text{-Br})(\text{S}_2\text{CN}^n\text{Bu}_2)_6(\text{C}\equiv\text{CPh})_4](\text{PF}_6)$, **4e**; and $[\text{Cu}_{12}(\mu_{12}\text{-Cl})(\mu_3\text{-Cl})(\text{S}_2\text{CN}^n\text{Bu}_2)_6(\text{C}\equiv\text{CCO}_2\text{Me})_3]^+$ **5a**. Cluster **1a** is the first structurally characterized copper cluster having a Cu_{13} centered cuboctahedral arrangement, a miniature of the bulk copper *fcc* structure. Furthermore, the partial $\text{Cu}(0)$ character in the 2-electron superatoms **1** was confirmed by XANES. Inverse coordination clusters **2–5** are the first examples of copper clusters containing main group elements (Cl, Br, S) with a hyper-coordination number, twelve. A combined theoretical and experimental study was performed, which shows that the central copper (formally Cu^{1-}) in nanoclusters **1** can be replaced by chalcogen/halogen atoms, resulting in the formation of clusters **2–5** which show enhanced luminescence properties and increase in the ionic component of the host–guest interaction as $\text{Br} \approx \text{Cl} > \text{S} > \text{Cu}$, which is consistent with the Cu-X Wiberg indices. The new compounds have been characterized by ESI-MS, ^1H , ^{13}C NMR, IR, UV-visible, emission spectroscopy, and the structures **2a–b**, **3d–e**, **4e** and **5a** were established by X-ray diffraction analysis.

Received 3rd April 2018
Accepted 30th June 2018

DOI: 10.1039/c8sc01508b

rsc.li/chemical-science

Introduction

The concept of inverse coordination, as recently defined by Haiduc,¹ applies to metal complexes in which the arrangement of acceptor and donor sites is opposite to that occurring in Werner-type coordination complexes. Inverse coordination complexes are formed around a non-metal species as the central atom (ion) surrounded by a number of metal atoms (ions) connected or not by internal bridging (intramolecular) linkers. Thus, discarding the nature of metal–metal interactions (if any), inverse coordination complexes can be simply viewed as transition-metal clusters (with or without metal–metal bonding) encapsulating a main-group anion.

In recent years, our group has developed the chemistry of anion-encapsulated Cu^{I} and Ag^{I} clusters bridged by dichalcogenolate ligands (dithiocarbamates and dichalcogenophosph(in)ates).² Various high-coordination numbers have been observed and rationalized for anions located at the centre of such d^{10} -metal clusters.³ For instance, cubic metal clusters containing an octa-coordinated encapsulated anion are known (Chart 1, left side).⁴ Nona-coordination of a halide or a chalcogenide, where the encapsulated anion lies at the center of an M_{11} pentacapped trigonal prism (Chart 1, middle), has also been shown to exist.^{4,5} Later, we reported the first example of a dodeca-coordinated iodide lying at the center of an Ag_{12}

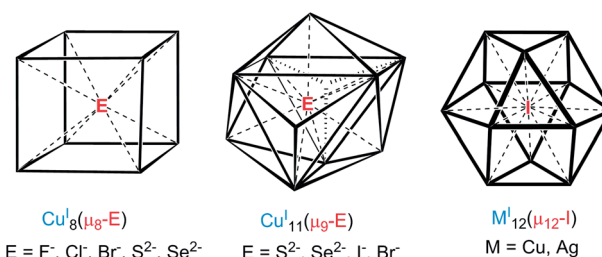


Chart 1 Geometries of hyper-coordinated chalcogen/halogen anions.

^aDepartment of Chemistry, National Dong Hwa University, No. 1, Sec. 2, Da Hsueh Rd. Shoufeng, Hualien 97401, Taiwan, Republic of China. E-mail: chenwei@mail.ndhu.edu.tw

^bUniv Rennes, CNRS, ISCR-UMR 6226, F-35000 Rennes, France

^cInstitute of Chemistry, Academia Sinica, Taipei 11528, Taiwan, Republic of China

^dNational Synchrotron Radiation Research Center, Hsinchu 30076, Taiwan

† Electronic supplementary information (ESI) available. CCDC 1501795, 1815418, 1815419, 1815421–1815424. For ESI and crystallographic data in CIF or other electronic format see DOI: 10.1039/c8sc01508b



cuboctahedron (Chart 1, right side).⁴ Lang and coworkers reported a cluster having a similar coordination environment for iodide in a cuboctahedral copper core.^{4b} It is worth noting that in the examples illustrated in Chart 1, no formal covalent bonding exists between the d¹⁰ metal centers, but only some metallophilic interactions.⁶

Understanding the mechanisms of nanocluster (NC) formation and reactivity is an important step toward the tailoring of new functional materials.¹ A substitution reaction is a typical chemical reaction where an atom or a functional group of a molecule is replaced by another atom or functional group.⁷

Compared to substitution reactions on a terminal ligand, substituting an inversely coordinated anion is much more difficult to perform due to the relatively high activation energy associated with this process.⁸ As far as we know, organometallic complexes with a main-group element in a very high coordination number have never been synthesized *via* the substitution reaction.

Recently, we reported the synthesis and characterization of a series of group 11 cuboctahedral metal NCs of the general formula $[\text{Cu}_{12}(\mu_{12}\text{-M})(\text{S}_2\text{CNR}_2)_6(\text{C}\equiv\text{CR}')_4]^+$ (M = Cu, Ag, Au).^{9a} In a first approximation, the bonding within these 2-electron superatoms can be described as resulting from the interaction of an encapsulated and formally M[−] anion with a cuboctahedral cage composed of twelve Cu^I ions. One fascinating query is whether it should be possible to substitute the encapsulated closed-shell M[−] anion by a closed-shell main-group anion, and further on, to replace this encapsulated main-group element by another one, the corresponding substitution reactions occurring without cluster disintegration.

Herein, we report the detailed synthesis and characterizations of chalcogen- and halogen-centred copper cuboctahedra. The compounds exhibit three distinct features: (1) the Cu₁₂ framework stabilized by both dithiocarbamate (dtc) and acetylide ligands is unprecedented; (2) the reported $\mu_{12}\text{-S}$ species are the very first compounds exhibiting a twelve-coordinated chalcogen encapsulated in a copper cluster; (3) the reported $\mu_{12}\text{-Cl}$ species constitute the only third example of a twelve-coordinated halogen in coordination chemistry.

Results and discussion

Synthesis and characterization

Previously we have demonstrated that the hydrides present in the copper(I) cluster $[\text{Cu}_{28}\text{H}_{15}(\text{dtc})_{12}]^+$ (dtc = di-*n*-butyldithiocarbamate = $\text{S}_2\text{CN}^n\text{Bu}_2$) react with the acidic protons of terminal alkynes to liberate molecular hydrogen, which subsequently reduces the excess of alkynes to alkenes, as well as parts of Cu^I to Cu⁰.^{9b} The generation of alkynyl ligands in the reaction medium leads eventually to the formation of a brand-new NC formulated as $[\text{Cu}_{13}(\text{dtc})_6(\text{alkynyl})_4]^+$ (**1**), which has a centered cuboctahedral $[\text{Cu}_{13}]^{11+}$ core possessing two 4s cluster electrons (1s² closed-shell configuration within the spherical jellium or superatom paradigm¹⁰). In a typical experiment, to a THF suspension of $[\text{Cu}_{28}\text{H}_{15}(\text{S}_2\text{CNR}_2)_{12}]^+$, a ten-fold excess of terminal alkyne was added and the reaction mixture was stirred at 30 °C for 24 hours. The solution undergoes a color change from orange to deep red, resulting in the deposition of a dark green solid. Workup of this mixture leads to the isolation of $[\text{Cu}_{13}\{\text{S}_2\text{CNR}_2\}_6\{\text{C}\equiv\text{CR}'\}_4](\text{PF}_6)$ (**1**) as a dark red solid in 40–70% yield (**1a** (70%): R = *n*Bu, R' = CO₂Me; **1b** (42%): R = *n*Bu, R' = CO₂Et; **1c** (65%): R = *i*Pr, R' = CO₂Et; **1d** (55%): R = *n*Pr, R' = 3,5-(CF₃)₂C₆H₃). In all the cases $[\text{Cu}_8\text{H}(\text{S}_2\text{CNR}_2)_6]^+$ and the corresponding alkene (methyl acrylate for **a**, ethyl acrylate for **b**, **c**, and 1,3-bis(trifluoromethyl)-5-vinylbenzene for **d**) have been isolated as byproducts. The hydrogen gas released from the reaction of the terminal alkyne's acidic hydrogen with the hydrides of $[\text{Cu}_{28}\text{H}_{15}(\text{S}_2\text{CNR}_2)_{12}]^+$ is assumed to be the reductant for the partial conversion of the alkyne to an alkene.

The positive-ion ESI mass spectrum of **1b–d** clearly displays a prominent band for the molecular ion $[\text{1b-PF}_6]^+$ at *m/z* 2438.6 (calcd 2438.7), $[\text{1c-PF}_6]^+$ at *m/z* 2270.3 (calcd 2270.5), $[\text{1d-PF}_6]^+$ at *m/z* 2830.3 (calcd 2830.4) and their simulated isotopic patterns match well with the experimental observations (Fig. 1a, S1 and S2†). As said above, with two 4s(Cu) electrons delocalized on its 13-atom metal core, the cluster cation **1** is a mixed-valent species, more precisely 2-electron superatoms.¹⁰ Notably, only a few 2-electron copper NCs are known: $[\text{Cu}_{25}\text{H}_{22}(\text{PPh}_3)_{12}]^+$, $[\text{Cu}_{29}\text{H}_{22}\text{Cl}_4(\text{Ph}_2\text{Phen})_{12}]^+$, and $[\text{Cu}_{20}(\text{CCPh})_{12}(\text{OAc})_6]$,^{11–13} and none of them has a cuboctahedral metal core.

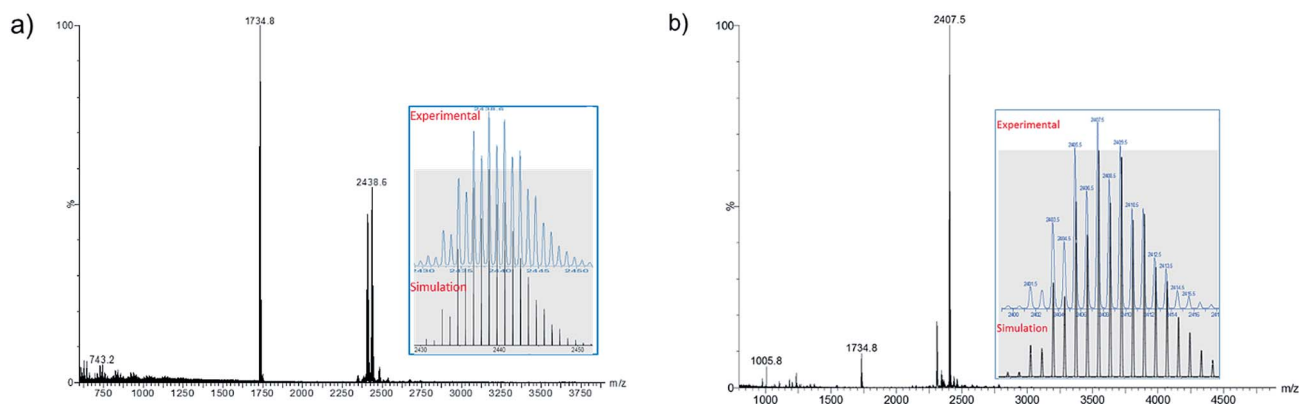


Fig. 1 Positive mode ESI-MS of **1b** (a) and **2b** (b). Insets: experimental and simulated mass spectra.



^1H and ^{13}C NMR spectra of **1a–d** show one set of signals, consistently with T_d symmetry in solution (see below). Their FT-IR spectra show that the alkynyl $\nu(\text{C}\equiv\text{C})$ stretching frequencies are lower than in the corresponding alkyne ($\nu(\text{HC}\equiv\text{CR}') = 2129\text{ cm}^{-1}$). **1a** shows a band at 2017.5 cm^{-1} . This value is slightly higher than in $[\text{Cu}_3(\mu\text{-dppm})_3(\mu_3\text{-}\eta^1\text{-C}\equiv\text{CCOO})(\mu_3\text{-OCH}_3)]$ (1976 cm^{-1}).¹⁴ The effect of Cu oxidation state(s) and cluster nuclearity is evident in the Cu K-edge X-ray absorption near-edge spectra (XANES) of **1a–d** (Fig. 2). At $\sim 8979.8\text{ eV}$, the edge position of **1a–d** is very similar to that of copper NCs, $[\text{Cu}_{29}\text{Cl}_4\text{H}_{22}(\text{Ph}_2\text{Phen})_{12}](\text{Cl})$ and $[\text{Cu}_{25}\text{H}_{22}(\text{PPh}_3)_{12}](\text{Cl})$ reported by Hayton^{11,12} and resides between values measured for Cu^0 in the bulk foil (8979.0 eV) and Cu^{I} in clusters such as $[\text{Cu}_{28}(\text{H})_{15}(\text{S}_2\text{CN}^n\text{Bu}_2)_{12}](\text{PF}_6)$ (8980.1 eV) and $[\text{Cu}_8(\text{H})(\text{S}_2\text{CN}^n\text{Bu}_2)_6](\text{PF}_6)$ (8980.3 eV). This is consistent with an average Cu oxidation state between 0 and +1 for **1a–d** (Table 1).

Compound **2a** has been synthesized by reacting **1a** with a two-fold excess of $\text{K}[\text{S}_2\text{CN}^n\text{Bu}_2]$ and the reaction mixture was stirred for 24 hours at 0°C (Scheme 1). The solution undergoes a color change from deep red to orange. Immediate workup of this mixture leads to the isolation of $[\text{SCu}_{12}(\text{S}_2\text{CN}^n\text{Bu}_2)_6(\text{C}\equiv\text{CCOOMe})_4]$ (**2a**) as a dark orange solid in 22% yield. Clusters **2b** and **2c** were isolated by following a similar synthetic procedure. The positive-ion ESI mass spectrum clearly displays

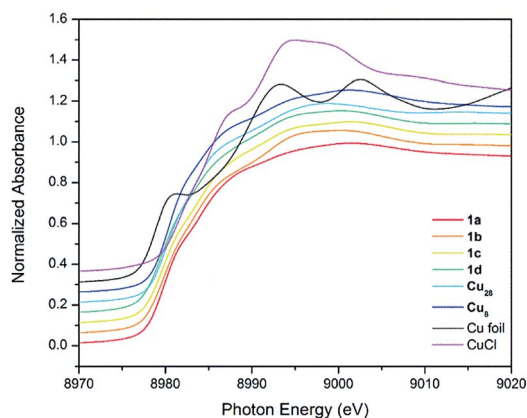
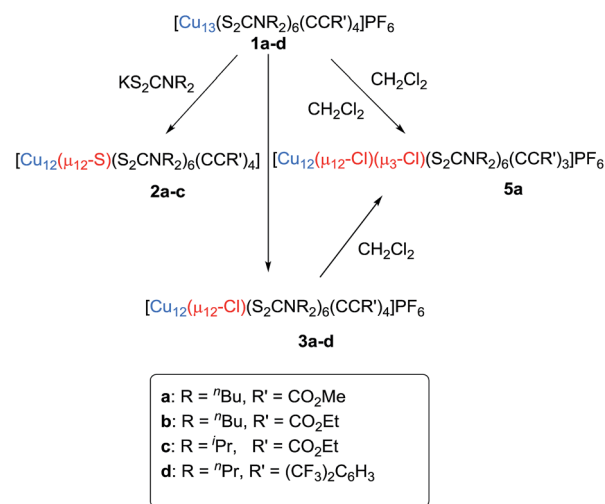


Fig. 2 Comparison of Cu K-edge XANES profiles for Cu foil, CuCl, copper(I) hydrides and NCs **1a–d**.

Table 1 Cu K-edge energies for selected Cu^0 and Cu^{I} species

Material	Edge (eV)
Cu foil	8979.0
$[\text{Cu}_{25}\text{H}_{22}(\text{PPh}_3)_{12}]\text{Cl}^{11}$	8979.6
$[\text{Cu}_{29}\text{Cl}_4\text{H}_{22}(\text{Ph}_2\text{Phen})_{12}]\text{Cl}^{12}$	8979.5
$[\text{Cu}_{13}(\text{S}_2\text{CN}^n\text{Bu}_2)_6(\text{C}_3\text{O}_2\text{Me})_4]\text{PF}_6$ (1a)	8979.8
$[\text{Cu}_{13}(\text{S}_2\text{CN}^n\text{Bu}_2)_6(\text{C}_3\text{O}_2\text{Et})_4]\text{PF}_6$ (1b)	8979.8
$[\text{Cu}_{13}(\text{S}_2\text{CN}^i\text{Pr}_2)_6(\text{C}_3\text{O}_2\text{Et})_4]\text{PF}_6$ (1c)	8979.8
$[\text{Cu}_{13}(\text{S}_2\text{CN}^n\text{Pr}_2)_6(\text{CF}_3)_2\text{C}_6\text{H}_3_4]\text{PF}_6$ (1d)	8979.7
Cu_2O	8980.0
$[\text{Cu}_{28}(\text{H})_{15}(\text{S}_2\text{CN}^n\text{Bu}_2)_{12}]\text{PF}_6$	8980.1
$[\text{Cu}_8(\text{H})(\text{S}_2\text{CN}^n\text{Bu}_2)_6]\text{PF}_6$	8980.3
$[\text{Cu}(\text{CH}_3\text{CN})_4]\text{PF}_6$	8980.3
CuCl	8981.6

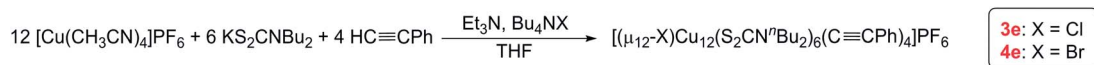
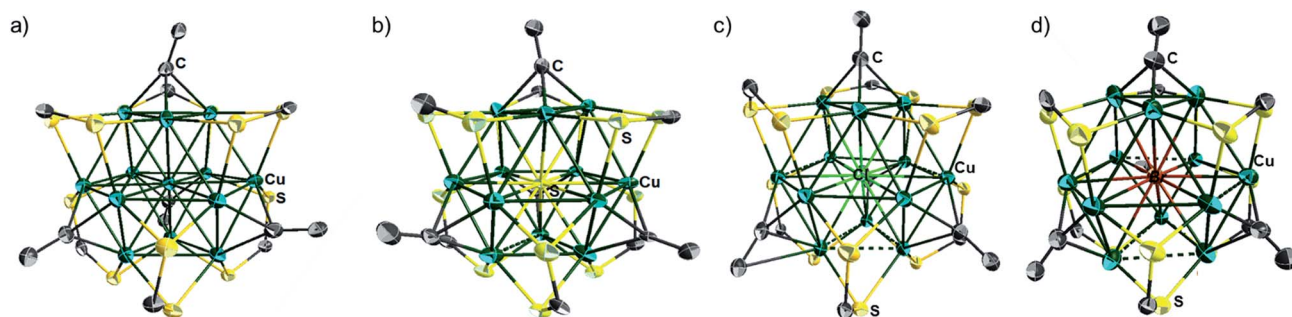


Scheme 1 Substitution reactions for the synthesis of compounds **2**, **3**, and **5** from **1**.

a prominent band for the molecular ion $[\mathbf{2a}]^+$ at m/z 2351.6 (calcd 2351.7), $[\mathbf{2b}]^+$ at m/z 2407.5 (calcd 2407.7), $[\mathbf{2c}]^+$ at m/z 2239.0 (calcd 2237.5), and their simulated isotopic patterns match well with the experimental observation (Fig. 1b, S3 and S4†). The presence of a sulfide atom in **2a–c** clearly originates from the dtc ligand. Indeed, the formation of S^{2-} from the sulfur-carbon bond cleavage in dtc ligands has been well documented.¹⁵

Compounds **3a–d** were isolated as yellow solids in 11–30% yield from the reaction of **1a–d** with dichloromethane for three days under ambient conditions. This reaction also produced $[\text{Cu}_{11}\text{Cl}_4(\text{S}_2\text{CNR}_2)_6]^+$ and a series of chloride-centred Cu_{12} cuboctahedral clusters with a different number of acetylide ligands $[\text{Cu}_{12}(\mu_{12}\text{-Cl})(\mu_3\text{-Cl})_n\{\text{S}_2\text{CNR}_2\}_6\{\text{C}\equiv\text{CR}'\}_{4-n}](\text{PF}_6)$ ($n = 1\text{--}3$), whose compositions were confirmed by ESI mass spectroscopy (Fig. S6 and S7†). This result suggests that three among the four acetylides of compound **3** can be replaced by halides. The geometric structure of $[\text{Cu}_{11}(\mu_9\text{-Br})(\mu_3\text{-Br})_3\{\text{S}_2\text{P}(\text{O}^i\text{Pr})_2\}_6]^+$.⁵ Separation of these compounds by column chromatography was difficult. However, we were lucky to grow single crystals of **5a** $[\text{Cu}_{12}(\mu_{12}\text{-Cl})(\mu_3\text{-Cl})\{\text{S}_2\text{CNR}_2\}_6\{\text{C}\equiv\text{CO}_2\text{Me}\}_3]^+$, which was characterized by X-ray crystallography (*vide infra*).

We have increased the yields in the production of compounds **3** by designing an alternative synthetic procedure. The direct synthesis involved the reaction of a terminal alkyne with a THF suspension of Cu^{I} salts and dtc ligands followed by the addition of few drops of triethylamine (Scheme 2). The reaction mixture was stirred at room temperature for ten minutes followed by the addition of tetrabutylammonium halide. The resulting solution was stirred for 12 hours, leading to the isolation of compounds **3e** and **4e** with 45% and 52% yields, respectively. The spectroscopic data of **3e** and **4e** are fully consistent with their X-ray structures described below (Fig. 3). The positive-ion ESI mass spectra clearly display a prominent band for the molecular ion $[\mathbf{3a}\text{-PF}_6]^+$ at m/z 2354.8 (calcd

Scheme 2 An alternative method for the synthesis of **3e** and **4e**.Fig. 3 Single crystal structures of the cluster cation **1a** (a), cluster **2a** (b), cluster cations of **3e** (c) and **4e** (d) with 30% thermal probability ellipsoids. All N^iBu_2 , $\text{C}(\text{O})\text{OMe}$ (**1a**, **2a**) and phenyl (**3e**, **4e**) moieties are omitted for clarity.

2354.7), $[\mathbf{3b}\text{-PF}_6]^+$ at m/z 2410.7 (calcd 2410.7), $[\mathbf{3c}\text{-PF}_6]^+$ at m/z 2242.5 (calcd 2240.5), $[\mathbf{3d}\text{-PF}_6]^+$ at m/z 2802.3 (calcd 2802.5), $[\mathbf{3e}\text{-PF}_6]^+$ at m/z 2426.4 (calcd 2426.8), and $[\mathbf{4e}\text{-PF}_6]^+$ at m/z 2470.5 (calcd 2470.7), and their simulated isotopic patterns match well with the experimental observation (Fig. 4 and S6–S9†).

FT-IR spectra of **3e** and **4e** show that the $\nu(\text{C}\equiv\text{C})$ stretching frequencies (2014, and 2015 cm^{-1} respectively) are lower than the values found for the corresponding alkyne ($\nu(\text{HC}\equiv\text{CPh}) = 2110 \text{ cm}^{-1}$).

In solution, ^1H NMR spectra for compounds **2a**, **3e** and **4e** were recorded at variable temperatures (183, 193, 243 and 273 K), which show only one set of ligands (in line with T_d symmetry, Fig. S10†). ^1H and ^{13}C NMR spectroscopic analyses of **5** show one set of ligands illustrating that the molecule is highly symmetric in solution. This is consistent with the ligand distribution pattern in **1**, implying their similarity in structure. Indeed, the ^1H chemical shifts of **1a** and **5a** are similar but their

integration ratios are different. Clusters **1–4** contain six dtc ligands and four alkynyl groups, whereas the ^1H NMR spectrum of **5a** shows the integration value of three alkynyl groups for six *n*-butyl dtc ligands. The replacement of one of the alkynyl groups with chloride is further confirmed by the ESI mass spectrum, where **5a** shows the molecular ion $[\mathbf{5a}]^+$ peak at m/z 2308.4 (calcd 2306.6) (Fig. S11†).

Structural analysis

The single-crystal X-ray structures of **1a**, **2a**, **2b**, **3d**, **3e** and **4e** are given in Fig. 3a, b, S5, S12,† 3c and d respectively. Corresponding relevant metrical data are given in Table 2. They all clearly show an X-centered Cu_{12} cuboctahedron (X = Cu (**1**), S (**2**), Cl (**3d**, **3e**), Br (**4e**)). The six square faces of the Cu_{12} cuboctahedron are capped by six dtc ligands, each of them bridging four metal centres in a (μ_2, μ_2) binding mode. As

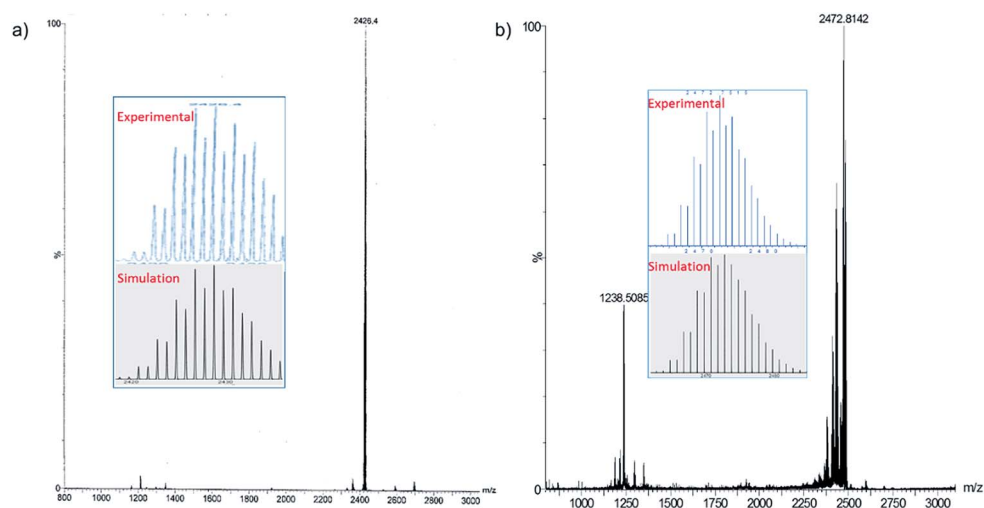
Fig. 4 Positive mode ESI-MS of **3e** (a), **4e** (b). The insets show experimental and simulated mass spectra.

Table 2 Selected bond lengths (Å) for **1a**, **2a–b**, **3d–e**, **4e** and **5a**

	X _{cent}	X _{cent} –Cu	Cu–Cu	C≡C	Cu _{cubo} –C	Cu _{cubo} –S
1a ⁹	Cu	2.605–2.669 Avg. 2.636	2.522–2.786 Avg. 2.636	1.187–1.213 Avg. 1.202	2.001–2.076 Avg. 2.035	2.257–2.320 Avg. 2.289
2a	S	2.589–2.934 Avg. 2.706	2.521–3.091 Avg. 2.709	1.179–1.220 Avg. 1.201	1.993–2.241 Avg. 2.094	2.256–2.328 Avg. 2.295
2b	S	2.561–2.892 Avg. 2.713	2.549–3.128 Avg. 2.717	1.143–1.200 Avg. 1.178	2.002–2.203 Avg. 2.092	2.264–2.359 Avg. 2.302
3d	Cl	2.694–2.957 Avg. 2.831	2.495–3.226 Avg. 2.844	1.222–1.223 Avg. 1.223	1.982–2.095 Avg. 2.019	2.206–2.332 Avg. 2.274
3e	Cl	2.807–3.035 Avg. 2.926	2.527–3.212 Avg. 2.884	1.205–1.257 Avg. 1.225	1.956–2.075 Avg. 2.025	2.243–2.291 Avg. 2.267
4e	Br	2.881–3.072 Avg. 2.977	2.563–3.306 Avg. 2.975	1.165–1.217 Avg. 1.190	1.943–2.100 Avg. 2.029	2.238–2.311 Avg. 2.269
5a	Cl	2.635–2.911 Avg. 2.778	2.563–3.245 Avg. 2.781	1.059–1.174 Avg. 1.134	1.985–2.173 Avg. 2.084	2.249–2.316 Avg. 2.279

a result, the twelve dtc sulfur atoms form a truncated tetrahedral cage. Four among the eight triangular faces of the cuboctahedron are capped by alkynyl groups in a $\mu_3\text{-}\eta^1$ fashion. It follows that each of the twelve outer Cu atoms is in an approximately planar CuS_2C coordination mode (not taking into account bonding with X). Not considering the substituents on alkynyls, the idealized symmetry of the clusters is T_d . The main-group-centered structures (**2a**, **b**, **3d**, **e** and **4e**) are however more distorted away from this ideal symmetry than that with $X = \text{Cu}$ (**1a**). This is exemplified by the larger dispersion of the Cu–Cu and X–Cu distances. All these structures exhibit one rather long X–Cu distance (Table 2) but still within bonding contacts (see below). The Cu–(μ_3 -S) bond lengths of **2a**, **b** are in the range 2.561(3)–2.934(4) Å, *i.e.* longer but comparable to that of Cu–(μ_9 -S) 2.402–2.870 Å in $[\text{Cu}_{11}(\mu_9\text{-S})(\mu_3\text{-Br})_3\{\text{S}_2\text{P}(\text{O}^i\text{Pr})_2\}_6]^{5a}$. The average Cu–(μ_{12} -Br) distance in **4e** (2.977 Å) is comparable to the Cu–(μ_9 -Br) distance (2.942 Å) observed in $[\text{Cu}_{11}(\mu_9\text{-Br})(\mu_3\text{-Br})_3\{\text{S}_2\text{P}(\text{O}^i\text{Pr})_2\}_6]^{+5}$. The average Cu–(μ_8 -X) distance in $[\text{Cu}_8(\mu_8\text{-X})\{\text{S}_2\text{P}(\text{O}^i\text{Pr})_2\}_4]^{+}$ is shorter than in **3d**, **e** and **4e** (2.72 (ref. 4c) and 2.74 Å (ref. 4d) for Cl and Br, respectively). The average Cu–Cu distances in compounds **2a–b**, **3d–e** and **4e** are larger than in the Cu-centered cluster **1a**, the largest value corresponding to the bromine-centered cluster **4e**, presumably owing to the larger size of bromine. In this particular compound, the Cu–Cu distance overpasses the sum of the van der Waals radii and it can be anticipated that the entrapment of anions larger than bromide into the Cu_{12} cage would destabilize the structure. For all the structures reported in Table 2, the Cu–S(dtc) Cu–C and C≡C bond distances (Table 2) are in the normal range and vary little across the series. The highest coordination number found in the literature is 8 for chloride and 9 for bromide.⁴ Thus, to the best of our knowledge, compounds **3d–e** and **4e** are the first isolated examples of μ_{12} -chloride and μ_{12} -bromide encapsulated in molecular compounds. In these clusters, as well as in the copper- and sulfide-centered species, the central atom plays a template role in the formation of this large cluster. This cuboctahedral configuration represents a marked contrast with the centered icosahedral geometry observed in the core unit of $[\text{Ag}_{20}\{\text{E}_2\text{P}(\text{O}^i\text{Pr})_2\}_{12}]$ (E = S, Se) and $[\text{Ag}_{21}\{\text{S}_2\text{P}(\text{O}^i\text{Pr})_2\}_{12}]^{+16}$. It is worth mentioning that no guest element exists in the

dodecahedral structures of $[\text{Cu}_{12}\text{S}_8]^{4-}$, $[\text{Cu}_{12}(\text{NPh})_8]^{4-}$, $[(^t\text{Bu}_3\text{-SiP})_6\text{Cu}_{12}]$, and $[\text{Cu}_{12}\text{E}_6(\text{PR}_3)_8]$ (E = S, Se, Te).¹⁷ Whereas a couple of examples of Au_{12} and Ag_{12} dodecahedra encapsulating a sodium or silver atom, respectively, are known,¹⁸ compounds **1–5** are the first examples of a copper cuboctahedron encapsulating another atom (except for Lang's compound of ref. 4h). In the case of **1a**, the metallic core is, to the best of our knowledge, the first example of a copper-centred Cu_{13} cuboctahedron, identical to that observed in the *fcc* structure of bulk copper.

The X-ray structure of **5a** (Fig. 5 and Table 2) can be derived from that of **3** by replacing one of the four μ_3 -alkynyl moieties by an isolobal $\mu_3\text{-Cl}$ ligand, which lowers the cluster ideal symmetry from T_d to C_{3v} . Apart from this substitution, the structure of **5a** is similar to that of clusters **3**. Not considering bonding with the encapsulated chloride, three among the twelve copper atoms are in the CuS_2C coordination, leaving nine other metals in a CuS_2C coordination. **5a** exhibits a broad range of Cu–Cu distances (2.563–3.245 Å). The corresponding average value (2.781 Å) is shorter than that observed in **3d** (2.844 Å). The average Cu–(μ_{12} -Cl) distance in **5a** (2.778 Å) is substantially larger than that corresponding to the Cu–(μ_3 -Cl) distance (2.321 Å). Interestingly, the C≡C distances of **5a** (avg. 1.134 Å) are significantly shorter than that of the tetra-alkynyl species reported in Table 2 (avg. 1.19–1.22 Å).

Optical properties

It is fascinating that a single atom alteration between clusters **1–3** can lead to diverse variances in their UV-vis spectra (Fig. 6). The homo-nuclear Cu_{13} cluster (**1a**) looks pinkish to the naked eye, whereas the sulfide- (**2a**) and chloride- (**3a**) centred clusters appear to be orange. The UV-vis spectrum of **1a** shows broad multiband optical absorption (at 337, 513, 540, 571 nm) and an intense absorption band at 287 nm, whereas the inverse coordination clusters **2a** (317, 450 nm) and **3a** (312 nm) show different patterns in their UV-vis spectrum. Substitution of the central metal atom (Cu) in **1** with main-group elements like sulfur and halogen increases the intensity of photoemission. At 77 K clusters **2a** and **3a** exhibit a structureless emission band, centred at 562 and 585 nm, respectively (Fig. S13†). On the other hand, the compound **1** is almost non-emissive.



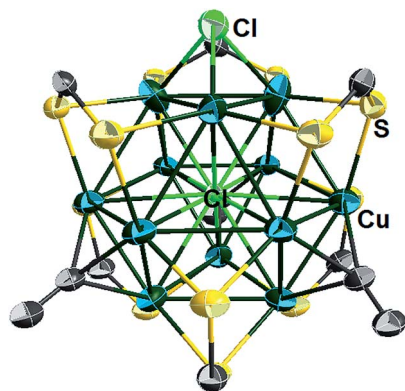


Fig. 5 Single crystal structure of the cluster cation **5a** with 30% thermal probability ellipsoids. All N^tBu_2 and $C(O)OCH_3$ moieties are omitted for clarity.

Theoretical investigations

In order to shed some light on the bonding and properties of the reported inverse-coordinated clusters, density functional theory (DFT) calculations were performed on various model clusters. The simplest homologs of compounds **1–4**, namely **1'–4'**, were built with $S_2CNR_2 = S_2CNH_2$ and $CCR' = CCH$. Relevant computed data are given in Table 3. The optimized geometries of **1'–4'** were all found to be of exact T_d symmetry (no imaginary

vibrational frequency). Their metrical parameters are in good agreement with the averaged experimental values of compounds **1–4** (Table 2). Unsurprisingly, the computed natural atomic orbital (NAO) charges are consistent with the formal oxidation state of the encapsulated element X being Cu^- , S^{2-} , Cl^- and Br^- in clusters **1'** to **4'**, respectively, whereas those of the 12 cuboctahedral metals always indicate the Cu^+ state. However, the differences between the computed and formal charges of X vary with its nature, indicating that the covalent component of the host-guest interaction decreases as $Cu > S > Br \approx Cl$. The Cu- X Wiberg indices (Table 3) are also consistent with this view. Thus **1'** ($X = Cu$) is substantially more covalent than **3'** ($X = Cl$). The simplified interaction diagrams of Fig. 7 illustrate this situation. Considering that each approximately planar tricoordinated Cu^I cuboctahedral vertex has a 4p vacant orbital pointing toward the middle of the cage, one is left with 12 vacant combinations ($a_1 + e + t_1 + 2t_2$) for the whole empty cage, of which the lowest ones ($a_1 + t_2$) constitute a nice set of accepting orbitals. In the case of $X = Cu$, the occupied 4s orbital of the encapsulated formally Cu^{I-} metal and the a_1 accepting orbital of the cage interact strongly, because of their proximity in energy. The resulting bonding a_1 MO is substantially delocalized on the 13 copper atoms and therefore both $Cu_{cent}-Cu_{cage}$ and $Cu_{cage}-Cu_{cage}$ bonding arise. This MO can be identified as the 1S jellium orbital¹⁰ containing the 2 electrons of the superatom **1'**.¹⁰ In the case of $X = Cl$, the occupied halide

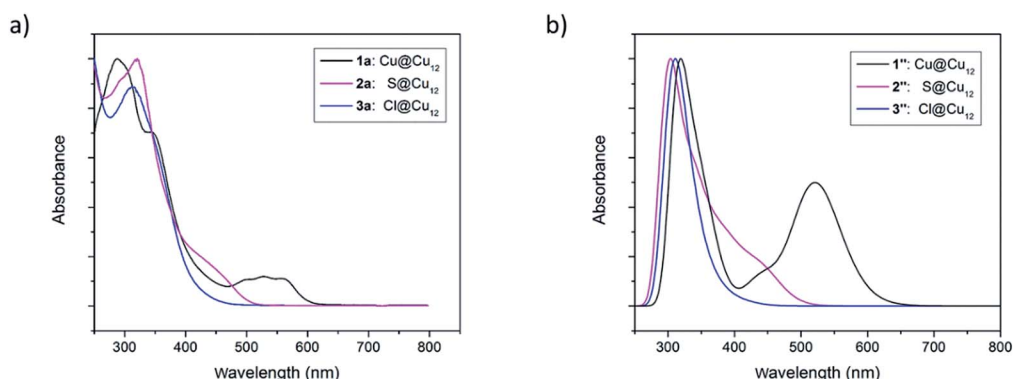


Fig. 6 (a) Experimental UV-vis absorption spectra of the clusters **1–3**. (b) TDDFT-simulated UV-vis absorption spectra of the clusters **1''–3''**.

Table 3 Selected computed data

	X	HOMO-LUMO gap (eV)	Cu- $X_{avg.}$ [range] ^a (Å)	WI(Cu- X) _{avg.} [range] ^b	Cu-Cu _{range} ^{a,b} (Å)	WI(Cu-Cu) _{range} ^c	$q(X)$ ^d	$q(Cu)_{avg.}$ ^{a,d}
1' (T_d)	Cu	3.08	2.666	0.061	2.595–2.725	0.047–0.050	−0.54	+0.69
1'' (C_1)	Cu	3.08	2.675 [2.637–2.722]	[0.047–0.074]	2.556–2.795	0.038–0.053	−0.53	+0.70
2' (T_d)	S	3.56	2.674	0.047	2.619–2.728	0.033–0.034	−1.61	+0.74
2'' (C_1)	S	3.53	2.747 [2.371–3.018]	0.049 [0.014–0.104]	2.532–3.276	0.008–0.048	−1.59	+0.75
3' (T_d)	Cl	3.84	2.899	0.023	2.707–3.085	0.019–0.036	−0.82	+0.75
3'' (C_1)	Cl	3.73	2.967 [2.721–3.271]	0.023 [0.012–0.049]	2.522–3.379	0.007–0.057	−0.81	+0.76
4' (T_d)	Br	3.82	2.942	0.026	2.708–3.168	0.015–0.036	−0.81	+0.75
5' (C_{3v})	Cl	3.72	2.931 [2.791–3.071]	0.024 [0.017–0.036]	2.719–3.133	0.012–0.040	−0.81	+0.74
6' (T_d)	Cl	4.07	2.971	0.026	2.829–3.111	0.039–0.054	−0.80	+0.70

^a Cu from the Cu_{12} cuboctahedron. ^b In the T_d symmetry, there are two symmetry-independent cuboctahedral Cu–Cu edges. ^c WI: Wiberg index. ^d q : Natural atomic charge.



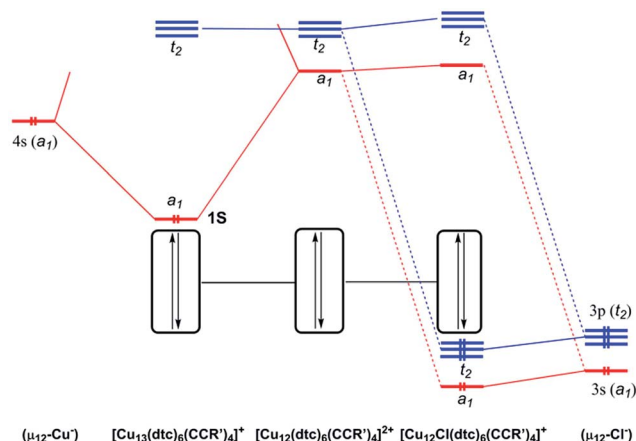


Fig. 7 Simplified MO interaction diagram illustrating the strength of the covalent interaction between the $[\text{Cu}_{12}(\text{dtc})_6(\text{CCR}')_4]^{2+}$ cage and its host: left: Cu^- , strong; right Cl^- , weak (ideal T_d symmetry assumed).

valence 3s and 3p orbitals can interact with the a_1 and t_2 accepting orbitals of the cage. However, because of the poor energy match between the interacting orbitals, the covalent interaction is weak. Thus, in the case of $\text{X} = \text{halogen or chalcogen}$, the host–guest bonding is dominated by its ionic component. Similar structural and bonding conclusions can be drawn for $5'$ (simplified model for 5a) and the hypothetical $[\text{Cu}_{12}(\mu_{12}\text{-Cl})(\text{dtc})_6\text{Cl}_4]^{2+}$ ($6'$).

In order to better reproduce the electronic properties of the experimental alkynyl ligands, models with $\text{CCR}' = \text{CC}(\text{COOH})$ were also computed, keeping $\text{dtc} = \text{S}_2\text{CNH}_2$. These models, namely $1''$, $2''$ and $3''$, were considered for $\text{X} = \text{Cu}$, S and Cl , respectively. Interestingly, the resulting optimized structures exhibited distorted geometries of C_1 symmetry (see Table 3). Whereas the distortion remains small in the case of $1''$, it is substantially larger for $2''$ and $3''$. This is exemplified by the large dispersion of the Cu-X distances in $2''$ and $3''$ ($\sim 2.4\text{--}3.0$ Å and $\sim 2.7\text{--}3.3$ Å, respectively), as compared to that in $1''$ ($\sim 2.6\text{--}2.7$ Å). Nevertheless, the averaged values computed for $1''\text{--}3''$ (Table 3) are very close to that of the symmetrical $1'\text{--}3'$ models. So are also the X NAO charges. It is noteworthy that the distortions away from ideal T_d symmetry afforded by $2''\text{--}3''$ are not equivalent to those exhibited by the clusters 2 and 3 reported in Table 2. These distortions appear rather random and likely result principally from steric and/or crystal packing forces in the investigated clusters. The fact that in solution clusters 2–4 show only one set of ligands (in line with T_d symmetry) at the NMR time scale is consistent with the primarily ionic character of the bonding between the encapsulated halide or chalcogenide and its $[\text{Cu}_{12}]^{12+}$ cage, as well as with the weak $\text{Cu}^+ \text{--} \text{Cu}^+$ interaction along the cuboctahedral edges. As a whole, our experimental and computed data indicate that clusters of the type 2–4 have a soft flexible shape resulting from the ionic, non-directed, nature of their host–guest interaction.

Time-dependent DFT (TD-DFT) calculations were performed to simulate the UV-vis spectra of clusters 1–3. Because of their high symmetry, the spectra obtained for the $1'\text{--}3'$ T_d models (Fig. S14†) are more structured than that of their $1''\text{--}3''$

homologs (Fig. 6b), the latter being thus closer to the experimental ones (Fig. 6a). The low-energy band observed for 1a at 540 nm is computed at 538 nm for $1'$ and corresponds to a HOMO (a_1)–LUMO (t_2) transition, a mixture of MMCT and MLCT ($\text{L} = \text{dtc}$) characters. As illustrated above in Fig. 7, the 1S HOMO present in $1'$ does not exist in the halide- or chalcogenide-centered species. Consequently, the latter cannot exhibit the same low-energy band. The band observed for 2a at 450 nm corresponds to a HOMO (t_2) \rightarrow LUMO (t_2) transition computed at 446 nm for $2'$. It is of MLCT ($\text{L} = \text{dtc}$) nature. A similar low-energy MLCT transition is computed at 390 nm for $3'$. For the three models, the major transitions of higher energy are mainly of MLCT character.

Conclusions

In summary, we have isolated and fully characterized $[\text{Cu}_{13}(\text{alkynyl})_4(\text{dtc})_6](\text{PF}_6)$ clusters, the first copper-centred cuboctahedral copper NCs, a miniature of the bulk copper *fcc* structure, with partial $\text{Cu}(0)$ character confirmed by XANES. Furthermore, they have been reacted to synthesize novel chalcogen- and halogen-centered cuboctahedral copper clusters $[\text{Cu}_{12}(\mu_{12}\text{-X})(\text{alkynyl})_4(\text{dtc})_6]^{2+}$ ($\text{E} = \text{Cl}$, Br , S). These clusters are the first examples of compounds in which a sulfide, chloride or bromide ion holds a so large coordination number (12). Prior to this report, the highest coordination number for sulfur and bromine was nine, and eight for chlorine. Bonding interactions between the Cu_{12} cuboctahedral cage and the encapsulated element (X), rationalized by DFT calculations, indicate that the covalent component of the host–guest bonding interaction decreases as $\text{Cu} > \text{S} > \text{Br} \approx \text{Cl}$. While the nature of the low-energy band observed for 1a can be reasonably assigned as a mixture of MMCT and MLCT ($\text{L} = \text{dtc}$) characters, it is primarily MLCT transition ($\text{L} = \text{dtc}$) for 2 and 3. Strikingly, new compounds have been prepared *via* replacing alkynyl with chloride. This synthetic methodology may open an avenue for the rational synthesis of organometallic compounds other than the spontaneous self-assembly. The new compounds synthesized are well characterized and the physical properties are explained by both theory and experimental methods.

Experimental section

General procedures and instrumentation

All chemicals were purchased from commercial sources and used as received. Solvents were purified following standard protocols. All reactions were performed in oven-dried Schlenk glassware using standard inert atmosphere techniques. All reactions were carried out in a N_2 atmosphere by using standard Schlenk techniques. $[\text{Cu}_{28}\text{H}_{15}(\text{S}_2\text{CN}^t\text{Bu}_2)_{12}]\text{PF}_6$ was prepared by a slightly modified procedure reported previously in the literature and characterized.¹⁹ NMR spectra were recorded on a Bruker Advance DPX300 FT-NMR spectrometer operating at 300 MHz. The chemical shift (δ) and coupling constant (J) are reported in ppm and Hz, respectively. ^{31}P NMR spectra were referenced to external 85% H_3PO_4 at δ 0.00. The ESI-mass spectrum was recorded on a Fison Quattro Bio-Q (Fisons



Instruments, VG Biotech, UK). XANES spectra at the Cu K-edge were recorded in transmission mode at beamline TLS-17C1 of the National Synchrotron Radiation Research Center (NSRRC), Taiwan. The electron storage ring was operated at 1.5 GeV with a beam current of 360 mA under top-up injection. A double-crystal Si(111) monochromator was employed for energy scanning. Incident and transmitted beam intensities were measured using gas-filled ionization chambers. An appropriate amount of each sample was adopted to reach the optimal thickness with the spectral edge jump being roughly unity. A standard Cu foil was measured simultaneously by using a third ionization chamber so that energy calibration could be performed scan by scan.

General synthetic method for the isolation of 1

In a flame-dried Schlenk tube, $[\text{Cu}_{28}(\text{H})_{15}(\text{S}_2\text{CNR}_2)_{12}](\text{PF}_6)$ (0.1 mmol) was suspended in THF (5 cm³) along with the terminal alkyne (1 mmol) and the resulting mixture was stirred at 30 °C for 24 h. The solvent was evaporated under vacuum and the residue was washed with diethyl ether (3 × 5 mL) to remove impurities from the ligand and the dark red residue was extracted in methanol. Finally, the solvent was evaporated to dryness under vacuum to get 1 as a pure powder in 40–70% yields. In this reaction, the corresponding alkene and $[\text{Cu}_8\text{H}(\text{S}_2\text{CNR}_2)_6]\text{PF}_6$ were produced as by-products.

$[\text{Cu}_{13}(\text{S}_2\text{CN}^n\text{Bu}_2)_6(\text{C}\equiv\text{CCOOEt})_4]\text{PF}_6$ (1b). (0.150 g, 42%, based on Cu): ESI-MS: m/z 2438.6 (M^+). ¹H NMR (300 MHz, CDCl₃): 4.15 (br, 8H, OCH₂), 4.02 (t, 24H, NCH₂), 1.79 (br, 24H, CH₂), 1.36 (br, 24H, CH₂CH₃), 1.27 (t, 12H, OCH₂CH₃), 0.94 (t, 36H, CH₃) ppm; ¹³C NMR (300 MHz, CDCl₃): 203.6, 152.7, 78.2, 74.8, 62.8, 52.1, 29.2, 20.1, 14.2, 13.7; ³¹P NMR (300 MHz, CDCl₃): −143.5 ppm; FT-IR data in KBr pellet (cm^{−1}): 2972.1, 1503, 942, 843.

$[\text{Cu}_{13}(\text{S}_2\text{CN}^i\text{Pr}_2)_6(\text{C}\equiv\text{CCOOEt})_4]\text{PF}_6$ (1c). (0.150 g, 65%, based on Cu): ESI-MS: m/z 2270.3 (M^+). ¹H NMR (300 MHz, CDCl₃): 5.96 (br, 6H, NCH), 4.18 (br, 6H, NCH), 3.95 (br, 8H, OCH₂), 1.63 (br, 36H, CH₃), 1.31 (br, 36H, CH₃), 1.29 (t, 12H, OCH₂CH₃) ppm; ¹³C NMR (300 MHz, CDCl₃): 201.2, 152.5, 78.5, 74.8, 62.6, 57.6, 20.5, 13.6; ³¹P NMR (300 MHz, CDCl₃): −143.5 ppm; FT-IR data in KBr pellet (cm^{−1}): 2961.1, 2931.7, 2872.7, 2009.1, 1594.0, 1498.4, 1233.3, 1143.2, 1080.0, 1027.5, 941.4, 835.3, 719.8, 557.2.

$[\text{Cu}_{13}(\text{S}_2\text{CN}^n\text{Pr}_2)_6\{\text{C}\equiv\text{CC}_6\text{H}_3(\text{CF}_3)_2\}_4]\text{PF}_6$ (1d). (0.150 g, 55%, based on Cu): ESI-MS: m/z 2830.3 (M^+). ¹H NMR (CDCl₃): 7.87 (br, 12H, ArH), 3.95 (br, 24H, NCH₂), 1.86 (br, 24H, CH₂CH₃), 0.96 (t, 36H, CH₃) ppm; ¹³C NMR (300 MHz, CDCl₃): 200.8, 132.7, 130.9, 123.3, 122.8, 88.5, 78.2, 55.7, 20.3, 12.2; ³¹P NMR (CDCl₃): −143.5 ppm; FT-IR data in KBr pellet (cm^{−1}): 2972.1, 1503, 942, 843.

General synthetic method for the isolation of 2

In a flame-dried Schlenk tube, $[\text{Cu}_{13}(\text{S}_2\text{CNR}_2)_6(\text{C}\equiv\text{CR}')_4](\text{PF}_6)$ (0.1 mmol) was suspended in THF (5 cm³) along with $\text{K}[\text{S}_2\text{CNR}_2]$ (0.22 mmol) and the resulting mixture was stirred at 0 °C for 24 h. The solvent was evaporated under vacuum and the desired compound was extracted in diethyl ether. Finally, the solvent

was evaporated to dryness under vacuum to get 2 as a pure orange powder in 20–30% yields.

$[\text{Cu}_{12}(\mu_{12}\text{-S})(\text{S}_2\text{CN}^n\text{Bu}_2)_6(\text{C}\equiv\text{CCOOMe})_4]$ (2a). ESI-MS: m/z 2351.6 (M^+). ¹H NMR (300 MHz, CDCl₃): 4.03 (t, 24H, NCH₂), 3.73 (s, 12H, OCH₃), 1.80 (br, 24H, CH₂), 1.40 (br, 24H, CH₂CH₃), 0.99 (t, 36H, CH₃) ppm; ¹³C NMR (300 MHz, CDCl₃): 203.4, 152.5, 96.6, 84.5, 54.2, 51.9, 28.8, 20.2, 14.0; FT-IR data in KBr pellet (cm^{−1}): 2962.2, 2937.2, 2874.3, 2015.1, 1694.3, 1502.3, 1297.7, 1218.2, 929.0, 845.3.

$[\text{Cu}_{12}(\mu_{12}\text{-S})(\text{S}_2\text{CN}^n\text{Bu}_2)_6(\text{C}\equiv\text{CCOOEt})_4]$ (2b). (0.150 g, 42%, based on Cu): ESI-MS: m/z 2407.5 (M^+). ¹H NMR (300 MHz, CDCl₃): 4.14 (br, 8H, OCH₂), 4.02 (t, 24H, NCH₂), 1.78 (br, 24H, CH₂), 1.37 (br, 24H, CH₂CH₃), 1.27 (t, 12H, OCH₂CH₃), 0.95 (t, 36H, CH₃) ppm; ¹³C NMR (300 MHz, CDCl₃): 203.8, 152.6, 78.5, 74.7, 62.7, 51.9, 28.9, 19.8, 14.4, 13.5; FT-IR data in KBr pellet (cm^{−1}): 2972.1, 1503, 942, 843.

$[\text{Cu}_{12}(\mu_{12}\text{-S})(\text{S}_2\text{CN}^i\text{Pr}_2)_6(\text{C}\equiv\text{CCOOEt})_4]$ (2c). (0.150 g, 65%, based on Cu): ESI-MS: m/z 2239.0 (M^+). ¹H NMR (300 MHz, CDCl₃): 5.92 (br, 6H, NCH), 4.10 (br, 6H, NCH), 3.92 (br, 8H, OCH₂), 1.69 (br, 36H, CH₃), 1.30 (br, 36H, CH₃), 1.26 (t, 12H, OCH₂CH₃) ppm; ¹³C NMR (300 MHz, CDCl₃): 200.7, 152.1, 78.8, 74.8, 62.3, 57.8, 21.2, 13.4; FT-IR data in KBr pellet (cm^{−1}): 2961.1, 2931.7, 2872.7, 2009.1, 1594.0, 1498.4, 1233.3, 1143.2, 1080.0, 1027.5, 941.4, 835.3, 719.8, 557.2.

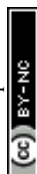
General synthetic method for the isolation of 3

In a flame-dried Schlenk tube, $[\text{Cu}_{13}(\text{S}_2\text{CNR}_2)_6(\text{C}\equiv\text{CR}')_4](\text{PF}_6)$ (0.1 mmol) was suspended in CH₂Cl₂ (5 cm³) and the resulting mixture was stirred at room temperature for 3 days. The solvent was evaporated under vacuum and the residue was washed with hexane, diethyl ether and methanol and the yellow residue was extracted in CH₂Cl₂. Finally, the solvent was evaporated to dryness and subjected to column chromatography to get 3 as a pure powder in 11–30% yields. Compound 5a was isolated as a byproduct in 5% yield.

An alternative method for the synthesis of 3e and 4e. In a flame-dried Schlenk tube, $[\text{Cu}(\text{CH}_3\text{CN})_4]\text{PF}_6$ (0.27 mmol) and $\text{K}[\text{S}_2\text{CN}^n\text{Bu}_2]$ (0.12 mmol) were suspended in 15 mL THF solvent. To this suspension HC≡CPh (0.08 mmol) and few drops of triethylamine were added and the reaction mixture was stirred at 0 °C for 10 minutes. To the reaction mixture, Bu₄NX (0.02 mmol) was added and stirred for 12 hours. The solvent was evaporated and the residue was washed with hexane, ether and methanol. The yellow residue was extracted in dichloromethane and purified by passing through alumina, which yielded 3e and 4e in 45 and 52% yields respectively.

$[\text{Cu}_{12}(\mu_{12}\text{-Cl})(\text{S}_2\text{CN}^n\text{Bu}_2)_6(\text{C}\equiv\text{CCOOMe})_4]\text{PF}_6$ (3a). ESI-MS: m/z 2354.8 (M^+). ¹H NMR (300 MHz, CDCl₃): 4.04 (t, 24H, NCH₂), 3.71 (s, 12H, OCH₃), 1.79 (br, 24H, CH₂), 1.41 (br, 24H, CH₂CH₃), 0.98 (t, 36H, CH₃) ppm; ¹³C NMR (300 MHz, CDCl₃): 203.7, 150.2, 98.2, 81.8, 51.7, 53.0, 29.2, 21.1, 13.4; ³¹P NMR (300 MHz, CDCl₃): −143.5 ppm; FT-IR data in KBr pellet (cm^{−1}): 2960.2, 2937.0, 2873.5, 2017.5, 1690.4, 1498.2, 1292.4, 1220.6, 928.5, 844.6.

$[\text{Cu}_{12}(\mu_{12}\text{-Cl})(\text{S}_2\text{CN}^n\text{Bu}_2)_6(\text{C}\equiv\text{CCOOEt})_4]\text{PF}_6$ (3b). (0.150 g, 42%, based on Cu): ESI-MS: m/z 2410.7 (M^+). ¹H NMR (300 MHz,



CDCl_3): 4.15 (br, 8H, OCH_2), 4.03 (t, 24H, NCH_2), 1.80 (br, 24H, CH_2), 1.37 (br, 24H, CH_2CH_3), 1.26 (t, 12H, OCH_2CH_3), 0.95 (t, 36H, CH_3) ppm; ^{13}C NMR (300 MHz, CDCl_3): 201.5, 153.5, 77.9, 74.5, 62.6, 52.0, 28.9, 20.2, 14.3, 13.3; ^{31}P NMR (300 MHz, CDCl_3): -143.5 ppm; FT-IR data in KBr pellet (cm^{-1}): 2972.1, 1503, 942, 843.

[Cu₁₂(μ_{12} -Cl)(S₂CNⁿPr₂)₆(C \equiv CCOOEt)₄]PF₆ (3c). (0.150 g, 65%, based on Cu): ESI-MS: m/z 2242.5 (M^+). ^1H NMR (300 MHz, CDCl_3): 5.95 (br, 6H, NCH), 4.16 (br, 6H, NCH), 4.10 (br, 8H, OCH_2), 1.65 (br, 36H, CH_3), 1.30 (br, 36H, CH_3), 1.28 (t, 12H, OCH_2CH_3) ppm; ^{13}C NMR (300 MHz, CDCl_3): 202.1, 151.6, 78.7, 74.5, 62.3, 57.5, 20.6, 13.7; ^{31}P NMR (300 MHz, CDCl_3): -143.5 ppm; FT-IR data in KBr pellet (cm^{-1}): 2961.1, 2931.7, 2872.7, 2009.1, 1594.0, 1498.4, 1233.3, 1143.2, 1080.0, 1027.5, 941.4, 835.3, 719.8, 557.2.

[Cu₁₂(μ_{12} -Cl)(S₂CNⁿPr₂)₆(C \equiv CC₆H₃(CF₃)₂)₄]PF₆ (3d). (0.150 g, 55%, based on Cu): ESI-MS: m/z 2802.3 (M^+). ^1H NMR (300 MHz, CDCl_3): 7.88 (br, 12H, ArH), 3.95 (br, 24H, NCH_2), 1.85 (br, 24H, CH_2CH_3), 0.98 (t, 36H, CH_3) ppm; ^{13}C NMR (300 MHz, CDCl_3): 199.8, 132.8, 131.6, 123.5, 123.0, 88.9, 78.6, 55.5, 20.2, 11.9; ^{31}P NMR (300 MHz, CDCl_3): -143.5 ppm; FT-IR data in KBr pellet (cm^{-1}): 2972.1, 1503, 942, 843.

[Cu₁₂(μ_{12} -Cl)(S₂CNⁿBu₂)₆(C \equiv CPh)₄]PF₆ (3e). ESI-MS: m/z 2426.4 (M^+). ^1H NMR (300 MHz, CDCl_3): 7.15–7.56 (m, 20H, C_6H_5), 3.81 (t, 24H, NCH_2), 1.62 (br, 24H, CH_2), 1.26 (br, 24H, CH_2CH_3), 0.82 (t, 36H, CH_3) ppm; ^{13}C NMR (300 MHz, CDCl_3): 202.5, 131.4, 128.1, 124.2, 59.4, 29.2, 20.4, 13.9; ^{31}P NMR (300 MHz, CDCl_3): -143.5 ppm; FT-IR data in CsI pellet (cm^{-1}): 2957.8, 2931.8, 2887.8, 2018.9, 1739.4, 1502.2, 1292.6, 1220.5, 926.8, 843.4.

[Cu₁₂(μ_{12} -Br)(S₂CNⁿBu₂)₆(C \equiv CPh)₄]PF₆ (4e). ESI-MS: m/z 2470.5 (M^+). ^1H NMR (300 MHz, CDCl_3): 7.15–7.56 (m, 20H, C_6H_5), 3.81 (t, 24H, NCH_2), 1.62 (br, 24H, CH_2), 1.26 (br, 24H, CH_2CH_3), 0.82 (t, 36H, CH_3) ppm; ^{13}C NMR (300 MHz, CDCl_3): 202.0, 131.6, 128.4, 124.2, 58.9, 28.8, 20.4, 14.2; ^{31}P NMR (300 MHz, CDCl_3): -143.5 ppm; FT-IR data in CsI pellet (cm^{-1}): 2959.4, 2932.0, 2889.2, 2020.4, 1739.6, 1502.2, 1292.6, 1220.6, 926.9, 843.4.

[Cu₁₂(μ_{12} -Cl)(μ_3 -Cl)(S₂CNⁿBu₂)₆(C \equiv CCOOMe)₃]⁺ (5a). ESI-MS: m/z 2308.4 (M^+). ^1H NMR (300 MHz, CDCl_3): 4.03 (t, 24H, NCH_2), 3.70 (s, 9H, OCH_3), 1.79 (br, 24H, CH_2), 1.39 (br, 24H, CH_2CH_3), 0.97 (t, 36H, CH_3) ppm; ^{13}C NMR (300 MHz, CDCl_3): 203.5, 150.7, 95.8, 82.7, 54.6, 51.8, 28.8, 21.2, 13.7; ^{31}P NMR (300 MHz, CDCl_3): -143.5 ppm; FT-IR data in KBr pellet (cm^{-1}): 2960.6, 2933.5, 2877.5, 2020.2, 1686.4, 1507.6, 1292.4, 1220.8, 928.7, 842.9.

X-ray structure determination

Single crystals suitable for X-ray diffraction analysis of **2a–b**, **3d–e**, **4e** and **5a** were obtained by slowly diffusing hexane into a concentrated dichloromethane/acetone solution at ambient temperature. The single crystals were mounted on the tip of glass fibre coated in paratone oil, then frozen. Data were collected on a Bruker APEX II CCD diffractometer using graphite monochromated Mo K α radiation ($\lambda = 0.71073$ Å) at 100 (**3d**, **3e**), 150 (**2a**, **5a**) and 296 (**2b**, **4e**) K. Data reduction was performed with SAINT.²⁰ Absorption corrections for the area

detector were performed by using the SADABS program.²¹ The structure was solved by direct methods and refined by least-squares against F^2 using the SHELXL-2018/3 package,²² incorporated in SHELXTL/PC V6.14.²³ All non-hydrogen atoms were refined anisotropically. Geometric restraints for the sp^3 carbon-carbon bond of these atoms were applied. In the crystal of **2a**, the C(O)OMe motifs on two of four methyl propiolate groups were disordered over two positions with equal occupancy. Structures **2b**, **3e** and **4e** contain large solvent-accessible voids, with substantial peaks of electron density visible inside these voids which could be due to the loss of solvent while mounting a single crystal at ambient temperature. In **3d**, the cocrystallization of $[\text{Cl}@Cu_{12}(\text{S}_2\text{CN}^n\text{Pr}_2)_6(\text{C}\equiv\text{CC}_6\text{H}_3(\text{CF}_3)_2)_4]\text{PF}_6$ and $[\text{Cu}@Cu_{12}(\text{S}_2\text{CN}^n\text{Pr}_2)_6(\text{C}\equiv\text{CC}_6\text{H}_3(\text{CF}_3)_2)_4]\text{PF}_6$ was found. The central atom in the Cu₁₂ cuboctahedral cage was refined with 70% Cl and 30% Cu. Cu1 and Cu1B are refined with occupancy ratio 0.7 : 0.3. Thus, the composition in crystal **3d** is $\{[\text{Cl}@Cu_{12}(\text{S}_2\text{CN}^n\text{Pr}_2)_6(\text{C}\equiv\text{CC}_6\text{H}_3(\text{CF}_3)_2)_4]\text{PF}_6\}_{0.7}[\text{Cu}@Cu_{12}(\text{S}_2\text{CN}^n\text{Pr}_2)_6(\text{C}\equiv\text{CC}_6\text{H}_3(\text{CF}_3)_2)_4]\text{PF}_6\}_{0.3}$. In **5a**, eight cationic $[\text{Cu}_{12}(\mu_{12}\text{-Cl})(\mu_3\text{-Cl})(\text{S}_2\text{CN}^n\text{Bu}_2)_6(\text{C}\equiv\text{CCOOMe})_3]^+$ molecules, four PF₆[−] anions, and four Cl[−] anions were found in one unit cell. The chloride atom was further disordered at multiple positions. Thus, the composition in crystal **5a** is $[\text{Cu}_{12}(\mu_{12}\text{-Cl})(\mu_3\text{-Cl})(\text{S}_2\text{CN}^n\text{Bu}_2)_6(\text{C}\equiv\text{CCOOMe})_3](\text{PF}_6)_{0.5}(\text{Cl})_{0.5}$. CCDC 1501795 (**1a**), 1815418 (**2a**), 1815419 (**2b**), 1815421 (**3d**), 1815422 (**3e**), 1815423 (**4e**) and 1815424 (**5a**) contain the ESI crystallographic data for this paper.†

Crystallographic data of **2a**: C₇₀H₁₂₀Cu₁₂N₆O₈S₁₃, orthorhombic, $P2_12_12_1$, $a = 18.2449(13)$ Å, $b = 23.2180(15)$ Å, $c = 23.3841(17)$ Å. $\alpha = 90^\circ$, $\beta = 90^\circ$, $\gamma = 90^\circ$. $V = 9905.7(12)$ Å³, $Z = 4$, ρ calcd = 1.578 cm^{-3} , $\mu = 2.840\text{ mm}^{-1}$, 56 212 measured reflections, 17 421 independent reflections ($R_{\text{int}} = 0.0477$), $R_1 = 0.0717$ [$I > 2\sigma(I)$], $wR_2 = 0.2124$ (all data), flack parameter: 0.05(3), goodness-of-fit on F^2 : 1.069. Crystallographic data of **2b**: C₇₄H₁₂₈Cu₁₂N₆O₈S₁₃, orthorhombic, $P2_12_12_1$, $a = 19.1023(9)$ Å, $b = 23.8001(11)$ Å, $c = 24.5421(12)$ Å. $\alpha = 90^\circ$, $\beta = 90^\circ$, $\gamma = 90^\circ$. $V = 11\,157.7(9)$ Å³, $Z = 4$, ρ calcd = 1.434 cm^{-3} , $\mu = 2.523\text{ mm}^{-1}$, 125 549 measured reflections, 19 663 independent reflections ($R_{\text{int}} = 0.0374$), $R_1 = 0.0490$ [$I > 2\sigma(I)$], $wR_2 = 0.1406$ (all data), flack parameter: -0.004(4), goodness-of-fit on F^2 : 1.043. Crystallographic data of **3d**: C₈₅H₁₀₂Cl_{0.7}Cu_{12.3}F₃₀N₆OPS₁₂, orthorhombic, $Pnna$, $a = 21.8103(5)$ Å, $b = 22.9770(6)$ Å, $c = 22.0395(6)$ Å. $\alpha = 90^\circ$, $\beta = 90^\circ$, $\gamma = 90^\circ$. $V = 11\,044.8(5)$ Å³, $Z = 4$, ρ calcd = 1.814 cm^{-3} , $\mu = 2.670\text{ mm}^{-1}$, 90 620 measured reflections, 9730 independent reflections ($R_{\text{int}} = 0.0303$), $R_1 = 0.0450$ [$I > 2\sigma(I)$], $wR_2 = 0.1122$ (all data), goodness-of-fit on F^2 : 1.099. Crystallographic data of **3e**: C₁₇₅H₂₆₂Cl₂Cu₂₄F₁₂N₁₂OP₂S₂₄, triclinic, $P\bar{1}$, $a = 17.6501(6)$ Å, $b = 19.8146(6)$ Å, $c = 32.8484(11)$ Å. $\alpha = 86.5157(9)^\circ$, $\beta = 89.7691(9)^\circ$, $\gamma = 75.7750(8)^\circ$. $V = 11\,114.5(6)$ Å³, $Z = 2$, ρ calcd = 1.555 cm^{-3} , $\mu = 2.561\text{ mm}^{-1}$, 83 631 measured reflections, 39 024 independent reflections ($R_{\text{int}} = 0.0260$), $R_1 = 0.0664$ [$I > 2\sigma(I)$], $wR_2 = 0.1885$ (all data), goodness-of-fit on F^2 : 1.107. Crystallographic data of **4e**: C₈₆H₁₂₈BrCu₁₂F₆N₆PS₁₂, triclinic, $P\bar{1}$, $a = 17.7551(15)$ Å, $b = 19.6625(17)$ Å, $c = 32.767(3)$ Å. $\alpha = 85.8425(17)^\circ$, $\beta = 85.6980(17)^\circ$, $\gamma = 76.1094(16)^\circ$. $V = 11\,055.9(16)$ Å³, $Z = 4$, ρ calcd = 1.573 cm^{-3} , $\mu = 2.911\text{ mm}^{-1}$, 63 677 measured reflections, 38 372 independent reflections ($R_{\text{int}} = 0.0533$), $R_1 =$



0.0806 [$I > 2\sigma(I)$], $wR_2 = 0.2652$ (all data), goodness-of-fit on F^2 : 1.047. Crystallographic data of **5a**: $C_{132}H_{234}Cl_5Cu_{24}F_6N_{12}O_{12}$ - PS_{24} , monoclinic, $C2/c$, $a = 31.396(3)$ Å, $b = 19.8294(17)$ Å, $c = 33.181(3)$ Å. $\alpha = 90^\circ$, $\beta = 97.8261(17)^\circ$, $\gamma = 90^\circ$. $V = 20\,465(3)$ Å³, $Z = 4$, ρ calcd = 1.557 cm^{-3} , $\mu = 2.804\text{ mm}^{-1}$, 56 963 measured reflections, 17 945 independent reflections ($R_{\text{int}} = 0.0445$), $R_1 = 0.0997$ [$I > 2\sigma(I)$], $wR_2 = 0.2334$ (all data), goodness-of-fit on F^2 : 1.015.

Computational details

Geometry optimizations were performed using DFT calculations with the Gaussian 09 package,²⁴ using the PBE0 functional²⁵ and the all-electron Def2-TZVPP set from EMSL Basis Set Exchange Library.²⁶ All the optimized geometries were characterized as true minima on their potential energy surface by harmonic vibrational analysis. The Wiberg bond indices were computed with the NBO 5.0 program.²⁷ The UV-visible transitions were calculated by means of TD-DFT calculations,²⁸ at the PBE0/Def2-TZVP level. Only singlet-singlet, *i.e.* spin-allowed, transitions were computed. The UV-visible spectra were simulated from the computed TD-DFT transitions and their oscillator strengths by using the SWizard program,²⁹ each transition being associated with a Gaussian function of half-height width equal to 1500 cm^{-1} . The compositions of the molecular orbitals were calculated using the AOMix program.³⁰

Conflicts of interest

There are no conflicts to declare.

Acknowledgements

This work was supported by the Ministry of Science and Technology in Taiwan (MOST 106-2113-M-259-010). The GENCI-CINES and GENCI-IDRISS French national computer centres are acknowledged for computational resources (grant x2016-087367).

Notes and references

- (a) I. Haiduc, *Coord. Chem. Rev.*, 2017, **338**, 1–26; (b) I. Haiduc, *Coord. Chem. Rev.*, 2017, **348**, 71–91.
- (a) C. W. Liu, H.-W. Chang, C.-S. Fang, B. Sarkar and J.-C. Wang, *Chem. Commun.*, 2010, **46**, 4571–4573; (b) C. Latouche, S. Kahlal, E. Furet, P.-K. Liao, Y.-R. Lin, C.-S. Fang, J. Cuny, C. W. Liu and J.-Y. Saillard, *Inorg. Chem.*, 2013, **52**, 7752–7765.
- (a) R. S. Dhayal, J.-H. Liao, Y.-R. Lin, P.-K. Liao, S. Kahlal, J.-Y. Saillard and C. W. Liu, *J. Am. Chem. Soc.*, 2013, **135**, 4704–4707; (b) C. W. Liu, B. Sarkar, Y.-J. Huang, P.-K. Liao, J.-C. Wang, J.-Y. Saillard and S. Kahlal, *J. Am. Chem. Soc.*, 2009, **131**, 11222–11233; (c) T. S. Lobana, J.-C. Wang and C. W. Liu, *Coord. Chem. Rev.*, 2007, **251**, 91–110.
- (a) J.-H. Liao, C. Latouche, B. Li, S. Kahlal, J.-Y. Saillard and C. W. Liu, *Inorg. Chem.*, 2014, **53**, 2260–2267; (b) Y. B. Chen, Z. J. Li, Y. Y. Qin, Y. Kang, J. K. Cheng, R. F. Hu, Y. H. Wen and Y. G. Yao, *Inorg. Chem. Commun.*, 2003, **6**, 405; (c) C. W. Liu, C. M. Hung, B. K. Santra, H. C. Chen, H. H. Hsueh and J. C. Wang, *Inorg. Chem.*, 2003, **42**, 3216–3220; (d) C. W. Liu, M. D. Irwin, A. A. Mohamed and J. P. Fackler Jr, *Inorg. Chim. Acta*, 2004, **357**, 3950–3956; (e) C. W. Liu, C. M. Hung, H. C. Haia, B. J. Liaw, L. S. Liou, Y. F. Tsai and J. C. Wang, *Chem. Commun.*, 2003, 976–977; (f) C. W. Liu, H. C. Haia, C. M. Hung, B. K. Santra, B. J. Liaw, Z. Y. Lin and J. C. Wang, *Inorg. Chem.*, 2004, **43**, 4464–4470; (g) C. W. Liu, *Phosphorus, Sulfur Silicon Relat. Elem.*, 2005, **180**, 923; (h) Z.-H. Wei, C.-Y. Ni, H.-X. Li, Z.-G. Ren, Z.-R. Sun and J.-P. Lang, *Chem. Commun.*, 2013, **49**, 4836–4838; (i) Y.-J. Li, C. Latouche, S. Kahlal, J.-H. Liao, R. S. Dhayal, J.-Y. Saillard and C. W. Liu, *Inorg. Chem.*, 2012, **51**, 7439–7441.
- (a) B. Li, J.-H. Liao, H.-T. Tang, Y.-J. Li and C. W. Liu, *Dalton Trans.*, 2013, **42**, 14384–14387; (b) C. Latouche, J.-H. Liao, Y.-J. Li, R.-Y. Shiu, V. Barone, S. Kahlal, C. W. Liu and J.-Y. Saillard, *Inorg. Chem.*, 2017, **56**, 14135–14146; (c) C. W. Liu, C.-M. Hung, B. K. Santra, Y.-H. Chu, J.-C. Wang and Z. Lin, *Inorg. Chem.*, 2004, **43**, 4306–4314.
- F. Scherbaum, A. Grohmann, B. Huber, C. Krgger and H. Schmidbaur, *Angew. Chem., Int. Ed. Engl.*, 1988, **27**, 1544–1546.
- (a) Y.-Q. Hu, M.-H. Zeng, K. Zhang, S. Hu, F.-F. Zhou and M. Kurmoo, *J. Am. Chem. Soc.*, 2013, **135**, 7901–7908; (b) X. Yang and M. B. Hall, *J. Am. Chem. Soc.*, 2007, **129**, 1560–1567.
- (a) S. J. Hilsenbeck, V. G. Young Jr and R. E. McCarley, *Inorg. Chem.*, 1994, **33**, 1822–1832; (b) X. Zhang and R. E. McCarley, *Inorg. Chem.*, 1995, **34**, 2678–2683.
- (a) R. P. B. Silalahi, K. K. Chakrahari, J.-H. Liao, S. Kahlal, Y.-C. Liu, M.-H. Chiang, J.-Y. Saillard and C. W. Liu, *Chem.-Asian J.*, 2018, **13**, 500–504; (b) K. K. Chakrahari, J.-H. Liao, S. Kahlal, Y.-C. Liu, M.-H. Chiang, J.-Y. Saillard and C. W. Liu, *Angew. Chem., Int. Ed.*, 2016, **55**, 14704–14708.
- (a) W. A. de Heer, *Rev. Mod. Phys.*, 1993, **65**, 611–675; (b) S. N. Khanna and P. Jena, *Phys. Rev. B: Condens. Matter Mater. Phys.*, 1995, **51**, 13705–13716; (c) M. Walter, J. Akola, O. Lopez-Acevedo, P. D. Jadzinsky, G. Alero, C. J. Ackerson, R. L. Whetten, H. Gronbeck and H. A. Hakkinen, *Proc. Natl. Acad. Sci. U. S. A.*, 2008, **105**, 9157–9162.
- T.-A. D. Nguyen, Z. R. Jones, B. R. Goldsmith, W. R. Buratto, G. Wu, S. L. Scott and T. W. Hayton, *J. Am. Chem. Soc.*, 2015, **137**, 13319–13324.
- T.-A. D. Nguyen, Z. R. Jones, D. F. Leto, G. Wu, S. L. Scott and T. W. Hayton, *Chem. Mater.*, 2016, **28**, 8385–8390.
- A. W. Cook, Z. R. Jones, G. Wu, S. L. Scott and T. W. Hayton, *J. Am. Chem. Soc.*, 2018, **140**, 394–400.
- H.-Y. Chao, L. Wu, B.-C. Su and X.-L. Feng, *Inorg. Chem. Commun.*, 2011, **14**, 122–124.
- G. Hogarth, *Prog. Inorg. Chem.*, 2005, **53**, 71.
- (a) R. S. Dhayal, J.-H. Liao, Y.-C. Liu, M.-H. Chiang, S. Kahlal, J.-Y. Saillard and C. W. Liu, *Angew. Chem., Int. Ed.*, 2015, **54**, 3702–3706; (b) R. S. Dhayal, Y.-R. Lin, J.-H. Liao, Y.-J. Chen, Y.-C. Liu, M.-H. Chiang, S. Kahlal, J.-Y. Saillard and



- C. W. Liu, *Chem.-Eur. J.*, 2016, **22**, 9943–9947; (c) W.-T. Chang, P.-Y. Lee, J.-H. Liao, K. K. Chakrahari, S. Kahlal, Y.-C. Liu, M.-H. Chiang, J.-Y. Saillard and C. W. Liu, *Angew. Chem., Int. Ed.*, 2017, **56**, 10178–10182; (d) Y.-R. Lin, P. V. V. N. Kishore, J.-H. Liao, S. Kahlal, Y.-C. Liu, M.-H. Chiang, J.-Y. Saillard and C. W. Liu, *Nanoscale*, 2018, **10**, 6855–6860.
- 17 (a) P. Betz, B. Krebs and G. Henkel, *Angew. Chem., Int. Ed. Engl.*, 1984, **23**, 311–312; (b) P. Reiß and D. Fenske, *Z. Anorg. Allg. Chem.*, 2000, **626**, 1317–1331; (c) N. Wiberg, A. Wörner, D. Fenske, H. Nöth, J. Knizek and K. Polborn, *Angew. Chem., Int. Ed.*, 2000, **39**, 1838–1842; (d) O. Fuhr, S. Dehnen and D. Fenske, *Chem. Soc. Rev.*, 2013, **42**, 1871–1906 and references cited therein.
- 18 (a) S.-P. Huang and M. G. Kanatzidis, *Angew. Chem., Int. Ed. Engl.*, 1992, **31**, 787–789; (b) V. G. Albano, L. Grossi, G. Longoni, M. Monari, S. Mulley and A. Sironi, *J. Am. Chem. Soc.*, 1992, **114**, 5708–5713.
- 19 P. V. V. N. Kishore, J.-H. Liao, H.-N. Hou, Y.-R. Lin and C. W. Liu, *Inorg. Chem.*, 2016, **55**, 3663–3673.
- 20 SAINT V4.043: Software for CCD Detector System, Bruker Analytic X-ray Systems, Madison, WI, 1995.
- 21 G. M. Sheldrick, *SADABS*, University of Göttingen, Göttingen, Germany, 1996.
- 22 G. M. Sheldrick, *Acta Crystallogr.*, 2015, **C71**, 3.
- 23 SHELXL v6.14 (PC version) Program Library for Structure Solution and Molecular Graphics, Bruker Analytical X-ray Systems, Madison, WI, 1998.
- 24 M. J. Frisch, G. W. Trucks, H. B. Schlegel, G. E. Scuseria, M. A. Robb, J. R. Cheeseman, G. Scalmani, V. Barone, B. Mennucci, G. A. Petersson, H. Nakatsuji, M. Caricato, X. Li, H. P. Hratchian, A. F. Izmaylov, J. Bloino, G. Zheng, J. L. Sonnenberg, M. Hada, M. Ehara, K. Toyota, R. Fukuda, J. Hasegawa, M. Ishida, T. Nakajima, Y. Honda, O. Kitao, H. Nakai, T. Vreven, J. A. Montgomery Jr, J. E. Peralta, F. Ogliaro, M. Bearpark, J. J. Heyd, E. Brothers, K. N. Kudin, V. N. Staroverov, R. Kobayashi, J. Normand, K. Raghavachari, A. Rendell, J. C. Burant, S. S. Iyengar, J. Tomasi, M. Cossi, N. Rega, J. M. Millam, M. Klene, J. E. Knox, J. B. Cross, V. Bakken, C. Adamo, J. Jaramillo, R. Gomperts, R. E. Stratmann, O. Yazyev, A. J. Austin, R. Cammi, C. Pomelli, J. W. Ochterski, R. L. Martin, K. Morokuma, V. G. Zakrzewski, G. A. Voth, P. Salvador, J. J. Dannenberg, S. Dapprich, A. D. Daniels, O. Farkas, J. B. Foresman, J. V. Ortiz, J. Cioslowski and D. J. Fox, *Gaussian 09, Revision E.01*, Gaussian, Inc., Wallingford CT, 2009.
- 25 (a) J. P. Perdew, M. Ernzerhof and K. Burke, *J. Chem. Phys.*, 1996, **105**, 9982–9985; (b) J. P. Perdew, M. Burke and M. Ernzerhof, *Phys. Rev. Lett.*, 1996, **77**, 3865–3868; (c) J. P. Perdew, K. Burke and M. Ernzerhof, *Phys. Rev. Lett.*, 1997, **78**, 1396.
- 26 F. Weigend and R. Ahlrichs, *Phys. Chem. Chem. Phys.*, 2005, **7**, 3297–3305.
- 27 E. D. Glendening, J. K. Badenhoop, A. E. Reed, J. E. Carpenter, J. M. Bohmann, C. M. Morales and F. Weinhold, Theoretical Chemistry Institute, University of Wisconsin, Madison, WI, 2001, <http://www.chem.wisc.edu/~nbo5>.
- 28 K. Burke and E. K. U. Gross, A guided tour of Time-Dependent Density Functional Theory, in *Density Functionals: Theory and Applications*, (Lecture Notes in physics), ed. D. Joubert, Springer, 1998, vol. 500.
- 29 S. I. Gorelsky, *SWizard program*, revision 4.5, <http://www.sg-chem.net/>.
- 30 S. I. Gorelsky, *AOMix program*, <http://www.sg-chem.net/>.

